

Light-Controlled Protein Dynamics Observed with Neutron Spin Echo Measurements

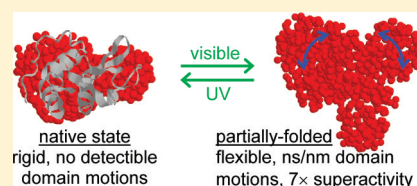
Shao-Chun Wang,[†] Panteha Mirarefi,[†] Antonio Faraone,^{‡,§} and C. Ted Lee, Jr.*[†]

[†]Department of Chemical Engineering and Materials Science, University of Southern California, Los Angeles, California 90089-1211, United States

[‡]Center for Neutron Research, National Institute of Standards and Technology, 100 Bureau Drive, Stop 6100, Gaithersburg, Maryland 20899-6102, United States

[§]Department of Materials Science and Engineering, University of Maryland, College Park, Maryland 20741, United States

ABSTRACT: A photoresponsive surfactant has been used as a means to control protein structure and dynamics with light illumination. This cationic azobenzene surfactant, azoTAB, which undergoes a reversible photoisomerization upon exposure to the appropriate wavelength of light, adopts a relatively hydrophobic, *trans* structure under visible light illumination and a relatively hydrophilic *cis* structure under UV light illumination. Small-angle neutron scattering (SANS) and neutron spin echo (NSE) spectroscopy were used to measure the tertiary structure and internal dynamics of lysozyme in the presence of the photosurfactant, respectively. The



SANS-based *in vitro* structures indicate that under visible light the photosurfactant induces partial unfolding that principally occurs away from the active site near the hinge region connecting the α and β domains. Upon UV exposure, however, the protein refolds to a nativelike structure. At the same time, enhanced internal dynamics of lysozyme were detected with the surfactant in the *trans* form through NSE measurements of the Q -dependent effective diffusion coefficient (D_{eff}) of the protein. In contrast, the D_{eff} values of lysozyme in the presence of *cis* azoTAB largely agree with the rigid-body calculation as well as those measured for pure lysozyme, suggesting that the native protein is dormant on the nanosecond time and nanometer length scales. Lysozyme internal motions were modeled by assuming a protein of two (α and β domains) or three (α and β domains and the hinge region) domains connects by either soft linkers or rigid, freely rotating bonds. Protein dynamics were also tracked with Fourier transform infrared spectroscopy through hydrogen–deuterium exchange kinetics, which further demonstrated enhanced protein flexibility induced by the *trans* form of the surfactant relative to the native protein. Ensemble-averaged intramolecular fluorescent resonance energy transfer measurements similarly demonstrated the enhanced dynamics of lysozyme with the *trans* conformation. Previous results have shown a significant increase in protein activity in the presence of azoTAB in the *trans* conformation. Combined, these results provide insight into a unique light-based method of controlling protein structure, dynamics, and function and strongly support the relevance of large domain motions for the activity of proteins.

Proteins are the building blocks of life and are responsible for a variety of functions, such as catalysis and transport. To properly function, a protein must adopt specific active conformations. However, proteins are not static entities and instead regularly undergo conformational rearrangements during the course of activity. For example, some enzymes exhibit a closed active site upon ligand–substrate binding and an open active site upon product release.^{1,2} Indeed, static images of proteins bound with a ligand began to emerge in the past decade, providing insight into the changes in protein conformation and internal dynamics required for protein function.³ However, static crystallographic structures provide protein dynamics averaged over hours.⁴ Proper examination of protein dynamics requires various techniques to cover the wide range of length scales and time scales of protein motions, from fast atomic local fluctuations to the relatively slow collective structural rearrangements of domain motions^{5,6} to the diffusive dynamics and folding process, this latter taking place on the microsecond to millisecond time scale. Nuclear magnetic resonance (NMR),^{7–11} dielectric relaxation spectroscopy,^{12–17} light,^{18–22} neutron,^{6,23} and X-ray²⁴ scattering are some of the techniques employed to investigate

different processes. Computer simulations have also been very important tools for studying such phenomena especially in combination with neutron scattering experiments.^{6,25–27} In addition, conformational flexibility has been examined by hydrogen–deuterium exchange and correlated with enzyme activity.^{28,29} Single-molecule measurements have further provided real-time observation of hidden dynamic events upon protein functioning.³⁰ Each of these techniques gives important insight into protein dynamics and an improved understanding of the protein structure–dynamics–function relationship.

Neutron spectroscopy is a scattering technique that allows investigation of both the time and length scale of the dynamical process on an atomic scale. Using different neutron scattering techniques, a dynamic range from the femtosecond to the microsecond can be covered.²³ In particular, neutron spin echo (NSE) allows the study of relaxational process taking place on length scales from a few to hundreds of angstroms and in a time

Received: February 9, 2011

Revised: August 1, 2011

Published: August 2, 2011

window from picoseconds to microseconds. These characteristics have been successfully employed for the investigation of microemulsions^{31–34} and polymers.^{34,35} In terms of protein dynamics, the application of neutron spectroscopy initially involved protein powders with low water content where translational and rotational motions could be neglected.³⁶ NSE has been used in the past to study the diffusive dynamics of protein solutions,^{37–41} whereas other quasielastic neutron scattering (QENS) techniques have been used to investigate the atomic motions on the angstrom scale in proteins.^{36,42–49} The atomic dynamics of membrane proteins and hydrated membrane stacks were investigated, as well.^{50–56} Time-resolved dynamic neutron scattering experiments were also performed to investigate on the angstrom scale how light affects dynamics in native photosystems.^{57,58} Inelastic neutron scattering was also used to study the light-induced vibrational and rotational dynamics in membranes of the photosynthetic bacterium *Rhodospseudomonas viridis*.⁵⁹

Recently, a DNA polymerase protein in D₂O solution has been investigated with NSE, revealing dynamics on the nanometer length scale associated with coupled interdomain motions, which are functionally important to the catalytic behavior of the enzyme.²⁶ The possibility of revealing and investigating such dynamical processes using NSE has been further demonstrated by an investigation of the dynamics of alcohol dehydrogenase.⁶⁰ This latter work clearly highlights the relevance of such dynamics for the functional activity of the enzyme. Very recently, NSE was used to investigate protein domain motions in NHERF1, a multidomain scaffolding protein,⁶¹ and phosphoglycerate kinase, an enzyme involved in the glycolytic pathway.⁶²

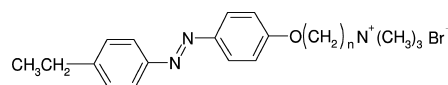
In previous studies, an azobenzene-based surfactant (azoTAB), which is in the relatively hydrophobic *trans* structure under visible light illumination and in the relatively hydrophilic *cis* structure under UV light illumination, was used to investigate the structure–function relationship of lysozyme.⁶³ SANS measurements indicated that in the presence of *trans* azoTAB the tertiary structure of lysozyme exhibits a higher degree of swelling primarily in the hinge region connecting the α and β domains, leading to an increase in the separation distance between the two domains relative to that of the protein in the presence of *cis* azoTAB, which exhibits a compact, nativelike structure. The swelling of the tertiary structure was accompanied by an approximately 7-fold enhancement in activity compared to the native protein as well as the *cis* azoTAB–protein complex.⁶³ At the time, it was hypothesized that enhanced protein internal dynamics, evidenced by the increase in the separation distance between the two protein domains in the ensemble-averaged SANS measurement, was the cause of the enzyme superactivity.

The goal of this work is to directly examine the effect of azoTAB and light illumination on the internal dynamics of lysozyme with neutron spin echo (NSE) spectroscopy. In this paper, new small-angle neutron scattering (SANS) measurements are reported, which provide the ensemble-averaged tertiary structure of lysozyme. In addition, H–D exchange kinetics were recorded to detect increases in protein flexibility using Fourier transform infrared (FT-IR) spectroscopy. Furthermore, ensemble-averaged fluorescent resonance energy transfer (FRET) measurements between a donor and acceptor dye located on opposite protein domains are examined to observe the effect of azoTAB on the tertiary structure and

dynamics of lysozyme. These complementary techniques give evidence of the ability of photosurfactants to control the complete form–dynamics–function relationship of proteins.

EXPERIMENTAL PROCEDURES

Materials. Highly purified lysozyme from hen egg white (L7651) and phosphate buffer (8.3×10^{-3} mol/L, pH 7.2) were purchased from Sigma and used as received. Azobenzene trimethylammonium bromide surfactants (azoTAB) of the form shown below were synthesized according to published procedures.⁶⁴ AzoTAB surfactants undergo a reversible photoisomerization upon exposure to the appropriate wavelength of light. Photoisomerization of the surfactant with light illumination changes the dipole moment across the $\text{N}=\text{N}$ bond. When it exists as the *trans* isomer, the surfactant has a lower dipole moment (planar structure) than the *cis* isomer (bent structure); thus, the *trans* isomer is more hydrophobic than the *cis* isomer. Under visible light, the surfactant exhibits a 75/25 *trans/cis* photostationary state, whereas with UV illumination, the surfactant exists primarily in the *cis* form (>90% *cis*). For H–D exchange kinetics observed with FT-IR, the $n = 2$ surfactant was used as described in previous lysozyme structural measurements,⁶⁵ while the $n = 4$ form used in previous lysozyme activity measurements⁶³ was used in all other experiments. Functionally, these two azoTAB molecules behave quite similarly, with the longer alkyl chain resulting in a slightly more hydrophobic molecule. Therefore, the $n = 4$ surfactant [critical micelle concentrations (CMCs) of 4.6×10^{-3} and 10.5×10^{-3} mol/L for *trans* and *cis* forms, respectively]⁶⁴ tends to have a higher binding affinity for proteins and to induce a higher degree of protein unfolding through hydrophobic interaction at lower surfactant concentrations compared to the $n = 2$ surfactant (*trans* and *cis* CMCs of 9.5 and 11.5 $\times 10^{-3}$ mol/L, respectively).⁶⁴



To collect FT-IR and fluorescence spectra, an azoTAB solution without protein was preconverted to the *cis* form using an 84 W long wave UV lamp at 365 nm (Spectroline, model XX-15A) prior to addition of the enzyme. For the neutron spin echo experiments, the protein/surfactant solution was illuminated with a 200 W mercury arc lamp (Oriel, model 6283) equipped with a 320 nm band-pass filter (Oriel, model 59800) in combination with a heat-absorbing filter (Oriel, model 59060), effectively isolating the 365 nm line (UV-A) to convert azoTAB to the *cis* form. During the period of FT-IR and NSE data collection, a liquid light guide (Oriel, model 77557) was attached to the arc lamp to continuously illuminate the sample with UV light to keep azoTAB in the *cis* state. The samples were inspected after each measurement to ensure that the surfactant remained in the *cis* state.

Small-Angle Neutron Scattering. The neutron scattering data were collected on the 30 m NG-3 SANS instruments at the National Institute of Standards and Technology (NIST) Center for Neutron Research (NCNR).⁶⁶ Two sample–detector distances were used (1.33 and 7.0 m), combined with a 25 cm offset of the detector, to give an exchanged momentum

transfer, Q , range of 0.0048–0.46 \AA^{-1} , where $Q = 4\pi\lambda^{-1} \sin(\theta/2)$ (θ is the scattering angle, and neutron wavelength λ was 6 \AA). The net intensities were corrected for the background (pure D_2O) and empty cell, followed by accounting for the detector efficiency using the scattering from an isotropic scatterer (Plexiglas), and then converted to absolute differential cross section per unit sample volume (in units of cm^{-1}) using an attenuated empty beam. The coherent scattering intensities of the sample were obtained by subtracting the incoherent contribution from the hydrogen atoms in lysozyme (0.004 cm^{-1}) and the surfactant ($\approx 0.002 \text{ cm}^{-1}$).

The SANS data were analyzed by calculation of the pair distance distribution functions (PDDFs) as well as a shape reconstruction algorithm. The PDDFs were calculated assuming a monodisperse system using GNOM⁶⁷ over a Q range of ≈ 0.02 – 0.3 \AA^{-1} to exclude effects of protein interactions at low Q values. The maximum particle diameter (D_{max}) was selected to give a smooth return of the PDDF to zero at D_{max} . The shape reconstructions were performed using GA_STRUCT supplied by W. Heller⁶⁸ with 1000 scattering centers used to represent the protein. A Q range of 0.01– 0.3 \AA^{-1} was employed to exclude potential protein interactions that would be exhibited at low Q and to avoid length scales too small for protein continuity at high Q values.

Neutron Spin Echo Experiments. NSE experiments were performed on the NG-5 neutron spin echo spectrometer at NIST⁶⁹ using a quartz sample cell with a 4 mm path length and a neutron incoming wavelength of 6 \AA . Using this wavelength, the accessible time range was from 50 ps to 15 ns, which would correspond, in the energy domain, to a resolution of $\approx 100 \text{ neV}$. This time range is appropriate for the study of the diffusional motion of lysozyme over a larger length scale and/or comparable with its size. The data were collected over a Q range of 0.046 \AA^{-1} to 0.2 \AA^{-1} at 25 °C. All samples were prepared with buffered D_2O solutions [$8.3 \times 10^{-3} \text{ mol/L}$ of sodium phosphate (pH 7.2)] to achieve a protein concentration of 10 g/L at varying surfactant concentrations. The data were corrected for the scattering from the solvent (D_2O buffer) and instrumental resolution effects to obtain normalized intermediate scattering functions $I(Q,t)/I(Q,0)$ at several wave vectors, Q . The DAVE software package was used for elements of data reduction and analysis.⁷⁰ Whereas a two-step decay of the intermediate scattering function has been reported in the case of alcohol dehydrogenase,⁶⁰ we did not find clear evidence of two relaxational processes, one related to the protein diffusional dynamics and one connected to the internal motions. Thus, the data were analyzed in terms of a single-exponential decay {in this case equivalent to the analysis of the first cumulant, the initial slope of the dynamic scattering function, $\Omega(Q) = -\partial \ln[I(Q,t)/I(Q,0)]/\partial t$, performed in previous similar studies^{26,60}} to determine the exchanged momentum transfer dependence of the effective diffusion coefficient of the protein, $D_{\text{eff}}(Q)$:

$$\frac{I(Q, t)}{I(Q, 0)} = \exp[-D_{\text{eff}}(Q)Q^2t] \quad (1)$$

Three models were employed to analyze the Q dependence of D_{eff} , including a rigid-body model (i.e., no domain motions), a soft linker domain model proposed by Bu et al.,²⁶ and a freely jointed domain model proposed by Akcasu et al.⁷¹ Each model is described in detail in the Appendix.

Kinetics of Hydrogen–Deuterium Exchange. All spectra were recorded with a Genesis II FT-IR spectrometer (Mattson Instruments) and a demountable liquid cell with a water-circulated jacket to control the temperature at 20 °C. For each time point, 100-scan interferograms were collected and averaged at a resolution of 4 cm^{-1} . The exchange was started by injecting buffered D_2O solutions [$8.3 \times 10^{-3} \text{ mol/L}$ of sodium phosphate (pH 7.2)] at varying azoTAB concentrations (in the range of 0– $1.2 \times 10^{-2} \text{ mol/L}$) into a vial containing an appropriate amount of lyophilized lysozyme to give a protein concentration of 10 g/L, followed by brief gentle mixing. The mixture was then immediately transferred to a demountable FT-IR liquid cell consisting of a pair of CaF_2 windows and a Teflon spacer (100 μm). Data collection started after a delay time of $\approx 2.5 \text{ min}$. A liquid light guide inserted into the FT-IR sample chamber was focused on the sample to introduce direct UV illumination throughout the data collection process for *cis* azoTAB–lysozyme complexes. Dried air was continuously purged into the chamber to eliminate the effect of water vapor. A set of reference spectra (buffered D_2O and azoTAB without protein) were collected under identical conditions, with the protein peaks in the amide I and amide II regions obtained by subtracting the corresponding reference spectra from the spectra of the protein solution. The fraction (F) of unexchanged hydrogen atoms in the protein was then determined by the ratio

$$F = \frac{\omega(t) - \omega(\infty)}{\omega(0) - \omega(\infty)} \quad (2)$$

where $\omega(t) = A_{\text{II}}(t)/A_{\text{I}}(t)$, with $A_{\text{II}}(t)$ and $A_{\text{I}}(t)$ representing the absorbance of amide II at $\approx 1542 \text{ cm}^{-1}$ and amide I at $\approx 1649 \text{ cm}^{-1}$, respectively, at time t . The value of $\omega(0)$ was obtained from a spectrum of undeuterated lyophilized lysozyme in KBr pellets. $\omega(\infty)$ was determined from protein samples aged for 10 days in D_2O at room temperature to ensure complete exchange. The protein sample without azoTAB required incubation at 37 °C to completely remove the amide II peak.

The H–D exchange kinetics of lysozyme at different azoTAB concentrations were analyzed with a multiexponential equation for i amide regions

$$F(t) = \sum_i a_i \exp(-k_i t) \quad (3)$$

where k_i represents the rate constant of different amide groups with similar exchange rates and a_i is proportional to the relative fraction of the i th region in the protein. The mean kinetic rate constant $\langle k \rangle$ was defined as⁷²

$$\langle k \rangle^{-1} = \frac{\sum_i a_i/k_i}{\sum_i a_i} \quad (4)$$

Fluorescence Resonance Energy Transfer (FRET) Spectroscopy. Wild-type T4 lysozyme was used for the FRET measurements, with the construct of the protein kindly provided by B. Matthews at the University of Oregon (Eugene, OR). Attachment of the donor (Alexa Fluor 532 maleimide) and acceptor (Alexa Fluor 594 maleimide) dyes to the two cysteine residues in the protein (Cys54 and Cys97, located on the β and α domains, respectively) was achieved by thiolation using the standard procedure provided by Molecular Probes. Briefly, the donor dye was slowly added to the protein solution

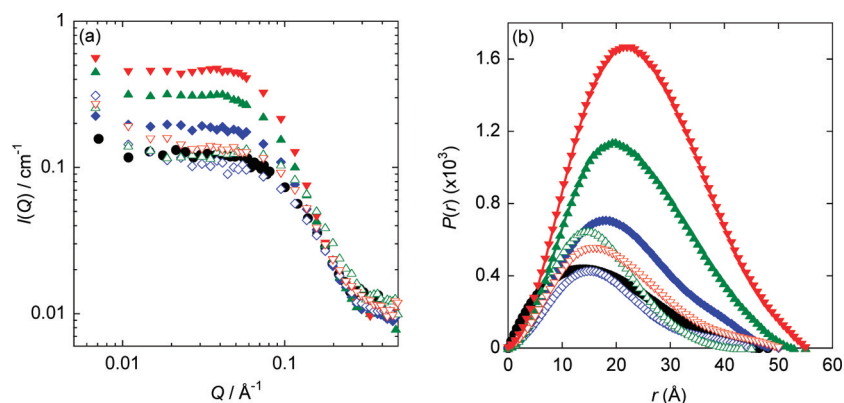


Figure 1. (a) SANS data and (b) PDDFs of lysozyme–azoTAB solutions as a function of surfactant concentration and light illumination (filled symbols for *trans* and empty symbols for *cis* azoTAB). Pure lysozyme (●), 5 mM azoTAB (blue symbols), 8 mM azoTAB (green symbols), and 12.0 mM azoTAB (red symbols) with 10 g/L lysozyme in pH 7.2 buffer.

(1 g/L) in phosphate buffer (20×10^{-3} mol/L, pH 7.2) at a dye/protein ratio of 1/1. The mixture was allowed to react overnight at 4 °C. Unreacted dye was then removed by extensive dialysis. The percentage of labeling was kept low to prevent double labeling of the same dye on one protein molecule. Donor dye-labeled protein was then separated from unlabeled protein by hydrophobic interaction chromatography (phenyl sepharose high performance, GE Healthcare) and further labeled with the acceptor dye with similar procedures. Approximately 90 and 70% of the product was labeled with the donor and acceptor, respectively, estimated via UV–vis spectroscopy.

The ensemble-averaged fluorescence of the protein was obtained by excitation at 510 nm. The emission spectra exhibited peaks of both the donor and acceptor at 544 and 617 nm, respectively, further confirming the success of the dye pair labeling. To observe the effect of azoTAB surfactant on FRET, 0.05×10^{-3} L of a 0.03 g/L protein solution and varying amounts of a concentrated surfactant solution were added to 0.9×10^{-3} L of phosphate buffer (8.3×10^{-3} mol/L, pH 7.2), resulting in a 1.6×10^{-3} g/L protein solution and the desired surfactant concentration (in the range of 0 – 0.14×10^{-3} mol/L). The relative ensemble-averaged FRET efficiency was evaluated using the equation $E_{ET} = I_A / (I_A + I_D)$, where I_A and I_D correspond to the fluorescence intensity of the acceptor at 617 nm and the donor at 544 nm, respectively, normalized by the efficiency of labeled protein in the absence of surfactant.⁷³

RESULTS AND DISCUSSION

SANS data for the lysozyme–azoTAB complexes as a function of azoTAB concentration and light conditions are shown in Figure 1. Similar to the case for lysozyme–azoTAB complexes at pH 5,⁶³ with increasing azoTAB concentrations the scattering curves under visible light shown in Figure 1a begin to deviate from pure lysozyme at $Q \approx 0.2 \text{ \AA}^{-1}$, which corresponds to a length scale $L (=2\pi/Q)$ of $\approx 30 \text{ \AA}$. Compared to the published value for the diameter of lysozyme ($\approx 35 \text{ \AA}$),^{65,74} this deviation suggests that azoTAB induces swelling of the lysozyme tertiary structure. In contrast, the scattering curves with *cis* azoTAB are almost identical to that of the pure protein, indicating the structure of lysozyme is not significantly influenced by *cis* azoTAB.

Radii of gyration (R_g) of lysozyme at different azoTAB concentrations and under different light conditions were

calculated from the SANS data by Guinier analysis (not shown) using the equation $I(Q) = I(0) \exp(-Q^2 R_g^2 / 3)$, where $I(0)$ is the extrapolated scattering intensity at $Q = 0$. The R_g values were observed to steadily increase with increasing azoTAB concentration under visible light [R_g values of 13.5, 15.2, 16.9, and 18.3 Å (error of <5%) with 0 , 5.0×10^{-3} , 8.0×10^{-3} , and 12.0×10^{-3} mol/L azoTAB, respectively]. Upon UV illumination, however, lysozyme apparently refolds to dimensions similar to those of native lysozyme [R_g values of 12.5, 12.9, and 13.5 Å (error of <5%) with 5×10^{-3} , 8×10^{-3} , and 1.2×10^{-2} mol/L azoTAB, respectively], supporting the notion that lysozyme is swollen by *trans*, but not *cis*, azoTAB.

The pair distance distribution functions (PDDFs) were calculated from the SANS data, as shown in Figure 1b. PDDFs represent the probability of finding two scattering centers within the protein a distance r apart. For globular proteins, the most probable distance between scattering centers (i.e., the maxima of the curves in Figure 1b) would then represent the radius of the protein, while the r values where the PDDFs return to zero would indicate the maximum dimension within the protein. With increasing *trans* azoTAB concentrations in Figure 1b, both the apparent protein radius and the maximum dimension shift to higher values, again indicating that *trans* azoTAB induces protein swelling. Upon conversion of azoTAB to the *cis* form with UV illumination, however, the protein refolds such that the apparent radius and maximum dimension return to values similar to those obtained for pure lysozyme.

Similar results are obtained by shape reconstruction analysis using GA_STRUCT.⁶⁸ As previously described for lysozyme,^{63,65} the program represents the protein as 1000 scattering centers, the positions of which are rearranged through a genetic algorithm to best fit the SANS data, providing an approximation of the *in vitro* protein conformation in solution. The shape-reconstructed lysozyme solution structures are displayed as red space-filling models in Figures 3 and 4. For the pure lysozyme solution, the analysis yields a protein structure that agrees well with the one reported by X-ray crystallography, as shown by the comparison with the crystallographic result in Figure 3a. On the other hand, in the case of the solution with azoTAB in the *trans* form, this analysis indicates a swelling of the structure, which increases with increasing surfactant concentrations (see shape-reconstructed images in Figure 4). In contrast, when azoTAB is in the *cis* form, the shape reconstruction analysis yields a structure largely similar to that found for pure lysozyme. The

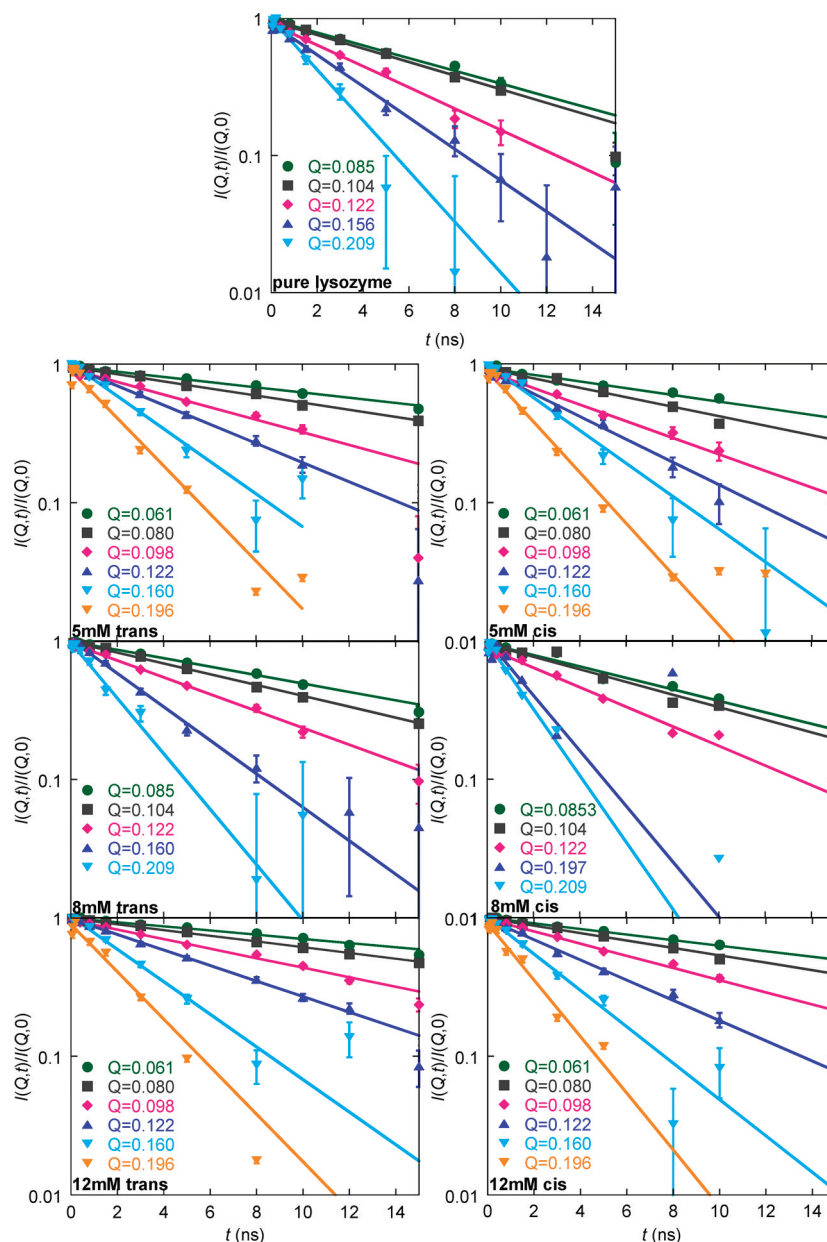


Figure 2. NSE data of azoTAB–lysozyme systems as a function of time t at representative Q values and surfactant concentrations and light conditions. Throughout the paper, error bars represent one standard deviation.

SANS data, analyzed using three different approaches, clearly show the ability to swell the lysozyme structure with azoTAB surfactant molecules when in the *trans* form and, at the same time, the possibility of switching off this phenomenon by the use of UV light with a *trans* to *cis* isomeric transition.

NSE data of the normalized intermediate scattering functions $I(Q,t)/I(Q,0)$ of lysozyme at representative Q values with different azoTAB concentrations and light conditions are shown in Figure 2. The data were fit with single-exponential decay functions as in eq 1, yielding the Q -dependent effective diffusion coefficients (D_{eff}) of lysozyme, as shown in Figures 3 and 4. For a perfectly spherical particle with no internal degrees of freedom, only the translational diffusion process will contribute to the decay of the intermediate scattering function and D_{eff} will be constant in Q . In the case of nonspherical molecules, the rotational motion would affect the measured diffusion coefficient, resulting in an increase in D_{eff} at Q values

corresponding to length scales similar to or larger than the particle dimension. The expected values of the effective diffusion coefficient as a function of Q , as determined by rigid-body translational and rotational motions, were calculated^{26,75} using the results of the shape reconstruction analysis and plotted as solid red lines in Figures 3 and 4. In the low- Q limit, the calculations compare well with the diffusion coefficient values obtained using dynamic light scattering (DLS). The NSE data of pure lysozyme shown in Figure 3a indicate that the measured effective diffusion coefficient agrees with these rigid-body calculations and oscillates around the low- Q translational diffusion coefficient collected by dynamic light scattering (solid blue data point placed at $Q = 0.05 \text{ \AA}^{-1}$), suggesting that the protein exists in the native form as a rigid structure on the nanosecond time scale and nanometer length scale. Furthermore, these rigid-body calculations from the SANS-based solution structure of pure lysozyme agree with

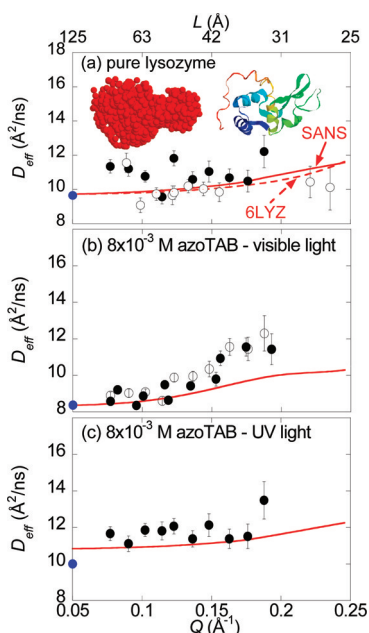


Figure 3. NSE data of the effective diffusion coefficient for (a) pure lysozyme and lysozyme with 8×10^{-3} mol/L azoTAB in the (b) *trans* and (c) *cis* conformations. In panel a, the ribbon diagram (PDB entry 6LYZ) represents the structure of lysozyme as obtained from crystallographic measurements, whereas the space-filling *in vitro* structure has been obtained from the SANS data. The solid blue data points at $Q = 0.05 \text{ \AA}^{-1}$ represent the center-of-mass translational diffusion coefficients obtained via DLS; the solid red lines represent rigid-body calculations (translation and rotation) using the SANS (solid red line) or crystal (6LYZ) (dashed red line) structures. Empty and filled symbols are used to denote data collected during separate visits to NIST.

those calculated from the lysozyme crystal structure [Protein Data Bank (PDB) entry 6LYZ, dashed red line], providing an additional level of confidence in the SANS-based solution structures.

As shown in Figure 3b, as an example of the case of lysozyme mixed with an azoTAB concentration of 8×10^{-3} mol/L, the NSE data show a deviation from the rigid-body calculations at Q values greater than 0.15 \AA^{-1} , corresponding to length scales on the order of the protein dimension. However, when the azoTAB conformation is changed from *trans* to *cis* with UV illumination, the rigid-body calculation again describes the experimental data with good accuracy in Figure 3c. These results indicate an enhancement of the internal dynamics of lysozyme in its partially unfolded state with respect to its native state due to surfactant denaturation. As previously suggested,⁶³ this increased mobility could be at the origin of the increased activity of the protein observed in the presence of azoTAB. The validity of this interpretation is supported by the fact that under UV illumination there is no sign of appreciable internal dynamics.

Figure 4 shows the effect of different azoTAB concentrations on lysozyme dynamics. At 5×10^{-3} mol/L azoTAB under visible light and up to 12×10^{-3} mol/L azoTAB under UV light, the experimental D_{eff} values largely agree with those predicted from rigid-body calculations, implying that the protein is not undergoing dynamic motions beyond translation and rotation [except perhaps for the deviations observed at Q values greater than 0.20 \AA^{-1} for 5×10^{-3} mol/L *trans* azoTAB and 12×10^{-3} mol/L *cis* azoTAB, which could denote

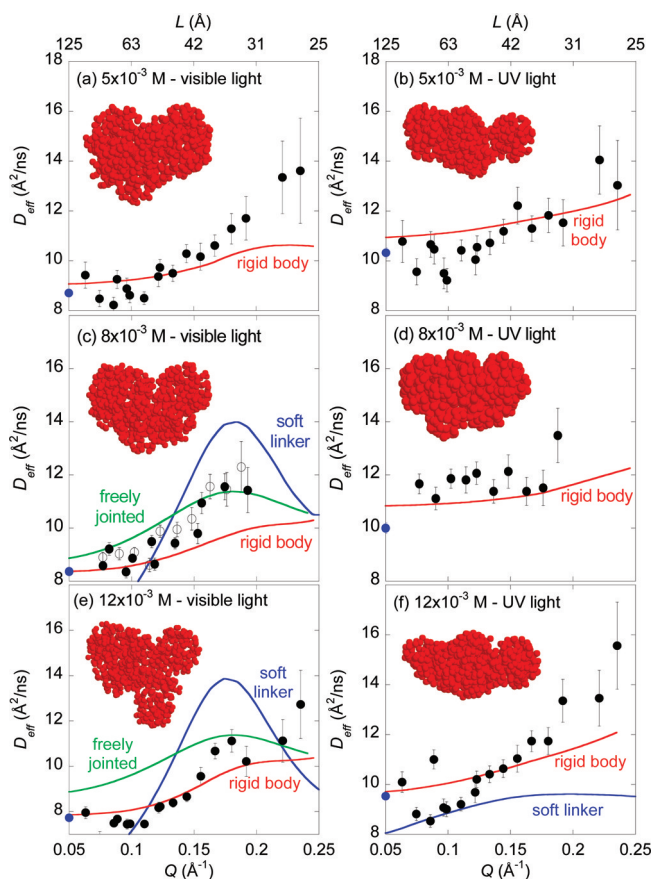


Figure 4. NSE data of lysozyme effective diffusion coefficients with (a) 5 (*trans*), (b) 5 (*cis*), (c) 8 (*trans*), (d) 8 (*cis*), (e) 12 (*trans*), and (f) 12 mM azoTAB (*cis*). The space-filling structure next to each plot represent the protein conformation at the corresponding azoTAB concentration. The solid blue data points at $Q = 0.05 \text{ \AA}^{-1}$ represent the center-of-mass translational diffusion coefficients obtained via DLS; the red lines represent rigid-body calculations using the SANS structures. The blue and green lines in panels c and e represent calculations using a soft linker domain model assuming two domains (blue lines) or a freely jointed domain model (green lines). Empty and filled symbols are used to denote data collected during separate visits to NIST.

the beginnings of the enhanced dynamics found with elevated azoTAB concentrations (see below)]. The effects of rotational motions are expected to become more pronounced as the protein becomes less globular. These results agree with the radii of gyration and maximum dimensions from the PDDF analysis of the SANS data, along with the shape-reconstructed lysozyme conformations obtained from the SANS data from Figure 2, which all indicate natively conformations of lysozyme under these conditions. Note that while large-scale deviations from rigid-body motions are not observed for these natively conformations, at elevated *cis* azoTAB concentrations a modest negative deviation in D_{eff} from a rigid body can be detected for Q values of $<0.12 \text{ \AA}^{-1}$, as well as positive deviation for Q values of $>0.2 \text{ \AA}^{-1}$, corresponding to a length scales of $\sim 30 \text{ \AA}$, smaller than the diameter of lysozyme (35 \AA). This suggests that the protein may perform small-scale internal motions under these conditions, albeit significantly fewer than the number observed under elevated *trans* azoTAB concentrations discussed below. For comparison, fluorescence measurements using the non-ionic, hydrophobic probe Nile red did indicate that lysozyme

was not as compactly folded as the native conformation at elevated *cis* azoTAB concentrations,⁶⁵ indicating a slight loosening of the protein hydrophobic core (although again significantly less than that observed with *trans* azoTAB). Thus, the relatively hydrophilic *cis* isomer of azoTAB may be beginning to induce slight protein unfolding at the highest surfactant concentrations studied.

In contrast, elevated concentrations of *trans* azoTAB (8×10^{-3} and 1.2×10^{-2} mol/L) are found to induce a pronounced deviation in D_{eff} from the rigid-body calculations at Q values around 0.15 \AA^{-1} , indicating that the protein performs large-scale motions under these conditions, possibly domain movements such as hinge bending motions or shear. The active site of lysozyme is located in a cleft between an α domain consisting mainly of α -helical segments and a β domain composed primarily of β -sheet structures. Connecting these two domains is a hinge region comprised of helix C, residues Glu35 and Ser36 on the loop succeeding helix B, and Ile55 and Leu56 at the turn between strands II and III.⁷⁶ To form a substrate–enzyme complex, it is well known that the protein has to perform hinge bending motions with the protein active site first opening (substrate-free state) and then closing (substrate-bound state). Indeed, X-ray crystallographic data of substrate-free T4 lysozyme revealed an active site more open than that of the substrate-bound form.⁷⁷ Single-molecule FRET measurements of T4 lysozyme also revealed hinge bending conformational changes related to protein function in real time.³⁰ From the SANS-based solution structures in Figures 3 and 4, the active site cleft can be observed in the top right of each molecule. With an increase in the concentration of *trans* azoTAB, the protein is observed to swell primarily in the hinge region at the bottom of the molecule, progressively resulting in a relatively open active site cleft, as observed in previous measurements.^{63,65} Thus, the ensemble SANS measurements are consistent with the protein exhibiting large-scale domain motions in solution.

Two models were applied to estimate the contributions of protein domain motions to the measured Q -dependent effective diffusion coefficients. The first model, proposed by Bu et al.,²⁶ treats the protein as separate rigid domains connected by soft spring linkers (see eq A2 in Appendix). Under the assumption that the protein is well within the overdamped soft spring regime, only the rotationally averaged static form factors of the domains and their friction constants need be considered and inertial modes as well as the recovering force from the connecting spring can be neglected. When this soft linker domain model is applied to lysozyme with 8×10^{-3} and 1.2×10^{-2} mol/L *trans* azoTAB, the results obtained by assuming two domains (α and β domains, blue line) exhibit a peak at $Q \approx 0.17 \text{ \AA}^{-1}$, as shown in panels c and e of Figure 4. The peak location concurs with the regions where large deviations in the measured D_{eff} values from the rigid-body model are seen, suggesting that these excess dynamics are a result of protein domain motions. However, the relatively large values of D_{eff} obtained for the soft linker domain model versus the experimental data indicate that without bond length constraints this model overpredicts the magnitude of the domain motions in lysozyme. Attempts to refine this model by representing lysozyme with three domains (α and β domains and the hinge region, not shown) further highlighted the deviation in model prediction versus experimental data (e.g., giving a peak at $D_{\text{eff}} = 18.1 \text{ \AA}^2/\text{ns}$ at $Q = 0.18 \text{ \AA}^{-1}$ at 1.2×10^{-2} mol/L *trans*

azoTAB). The soft linker domain model is able to predict the negative deviation in the D_{eff} values from the rigid-body model at $Q \approx 0.1 \text{ \AA}^{-1}$ in the lysozyme system containing 1.2×10^{-2} mol/L *cis* azoTAB, suggesting that this deviation is a measurable effect of domain motions. However, for this only slightly unfolded lysozyme conformation, the soft linker domain model gives a weak maximum that underpredicts the D_{eff} values at elevated Q values. This latter effect is likely due to the beginnings of enhanced lysozyme dynamics occurring with elevated *cis* azoTAB concentrations.

Therefore, to take into account the effect of interdomain contacts, a freely jointed domain model⁷¹ (eq A4 in Appendix) was also used to describe the observed dynamics as shown in panels c and e of Figure 4, treating the protein as three rigid domains (α and β domains and the hinge region) connected with two freely jointed bonds of a constant length. The results show a similar increase in the dynamics at $Q \approx 0.175 \text{ \AA}^{-1}$, although in this case with more realistic values of D_{eff} throughout the entire Q range relative to the experimental data. This suggests that freely jointed domains better model the domain motions within lysozyme in the presence of *trans* azoTAB compared to domains connected by soft spring linkers, although it should be pointed out that even the freely jointed domain model overpredicts the D_{eff} values in the Q range from 0.05 to 0.1 \AA^{-1} (or at length scales on the order of 100 \AA). This is to be expected as the internal motions within lysozyme are much more complex than those represented by the freely jointed domain model, which assumes a polymer-like chain with identically sized beads (domains) and bond lengths. Furthermore, the assumption of freely rotating bonds without a constraint on the bond angle likely oversimplifies the domain motions with lysozyme. For example, with the α domain–hinge– β domain bond angle fully stretched to 180° , this model would allow lysozyme lengths of $\approx 110 \text{ \AA}$ (i.e., three 20 \AA domains connected by two 25 \AA bonds), twice the value of the maximum dimension ($\approx 55 \text{ \AA}$) measured from the PDDFs in Figure 1b. Thus, it is not surprising that this model would overpredict the D_{eff} values in the lower Q range in Figure 4 (i.e., $2\pi/110 \text{ \AA} \approx 0.05 \text{ \AA}^{-1}$).

Nevertheless, in the region of maximum deviation from the rigid-body calculations, the freely jointed domain model more accurately represents the domain motions within lysozyme relative to the soft linker domain model. These results should be contrasted with NSE measurements on DNA polymerase I from *Thermus aquaticus* (*Taq* polymerase), where the soft linker domain model was found to accurately model the protein domain motions evident in the NSE data.²⁶ Similar to lysozyme, *Taq* polymerase consists of two distinct domains (DNA polymerase domain and a 5'-nuclease domain) connected by a hinge region, with interdomain movements on the order of 9.8 \AA occurring upon substrate binding compared to 8 \AA for lysozyme. Thus, on first pass, similar domain motions might be expected in the NSE measurements of the two proteins. However, this is clearly not the case as native lysozyme was observed to be dormant on the nanosecond time and nanometer length scales in Figure 3, in stark contrast to *Taq* polymerase. Indeed, it is only upon swelling of the hinge region in the presence of *trans* azoTAB that domain motions can be detected within lysozyme with NSE. Lysozyme is a small, relatively rigid protein (129 residues containing four disulfide bonds), while *Taq* polymerase (831 residues) exists in an extended conformation with the polymerase and 5'-nuclease domains separated by $\approx 70 \text{ \AA}$. Furthermore, the

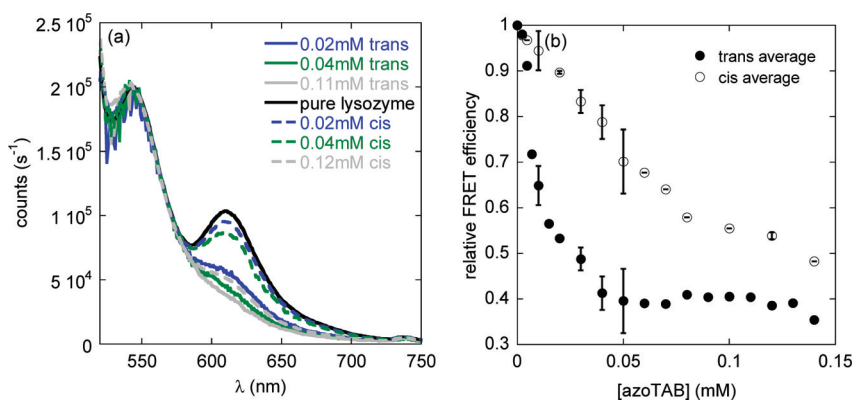


Figure 5. (a) Ensemble-averaged fluorescence spectra of Alexa 532- and Alexa 594-labeled T4 lysozyme with varying concentrations of azoTAB. (b) Ensemble-averaged FRET efficiency as a function of azoTAB concentration.

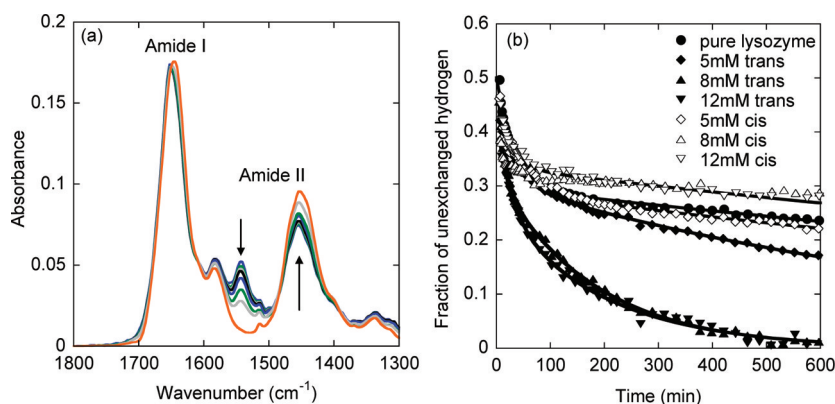


Figure 6. (a) Representative lysozyme H–D exchange spectra in the time range of 5 min to 10 h at 20 °C. Arrows in the spectra indicate the direction of peak intensity changes. The azoTAB concentration was 8 mM. (b) H–D exchange kinetics of lysozyme as a function of azoTAB concentration and light illumination (filled symbols for *trans* azoTAB and empty symbols for *cis* azoTAB). Pure lysozyme (●), 5 mM azoTAB (◆ and ◇), 8 mM azoTAB (▲ and △), and 12.0 mM azoTAB (▼ and ▽). The lysozyme concentration was 10 g/L in pH 7.2 buffer.

polymerase domain of *Taq* polymerase contains three subdomains that also undergo subdomain motion. Thus, overall it is not surprising that weaker domain motions are observed in lysozyme than in *Taq* polymerase.

To examine the effects of azoTAB on lysozyme conformation and dynamics, we recorded ensemble-averaged fluorescence resonance energy transfer (FRET) spectra (shown in Figure 5a). T4 lysozyme was labeled with one donor or acceptor dye at Cys54 (located near the hinge) and Cys97 (located in the α domain), positions sensitive to domain motions³⁰ and in the proximity of residues Ile55 and Leu56 in the hinge region.⁷⁶ Lysozyme from bacteriophage T4 is slightly larger, although similar in structure and function to hen egg white lysozyme of the type used in the SANS and NSE measurements. The dye-labeled pure protein excited at 520 nm exhibits an emission peak of the donor (Alexa Fluor 532) at 554 nm and the acceptor (Alexa Fluor 594) at 617 nm. Addition of azoTAB to the protein solution decreases the magnitude of the acceptor emission peak, indicating that the ensemble-averaged distance between the donor and acceptor increases. The relative FRET efficiency (see Experimental Procedures) was evaluated from these spectra as a function of azoTAB concentration, as shown in Figure 5b. With increasing concentrations of *trans* azoTAB, the FRET efficiency exhibits a dramatic decrease even at very low surfactant concentrations [e.g., 0.005×10^{-3} mol/L, or a surfactant/protein ratio (S/P) of 59/1] and reaches a constant value at a surfactant concentration of $\approx 0.05 \times 10^{-3}$ mol/L. In contrast, a slow and steady decrease in

FRET efficiency is induced by *cis* azoTAB. Although these surfactant concentrations seem low relative to the previous data, the S/P values in the FRET experiment are slightly higher than those used in SANS and NSE experiments (e.g., S/P = 18/1 at 12×10^{-3} mol/L azoTAB), a result of the relatively low protein concentration required in FRET experiments. The large and steady loss of FRET efficiency upon addition of surfactant is consistent with the swelling of the hinge region observed in the SANS-based in vitro conformations, indicating that the distance between Cys54 (located near the hinge) and Cys97 (located in the α domain) has increased.

To further examine the effect of azoTAB on lysozyme flexibility, H–D exchange kinetics of lysozyme with different azoTAB concentrations were collected with FT-IR spectroscopy. H–D exchange has been used to monitor protein dynamics, flexibility, and stability.^{72,78–80} Figure 6a shows a representative H–D exchange spectrum of lysozyme with 8×10^{-3} mol/L *trans* azoTAB. The replacement of amide protons (N-H) with deuterium (N-D) results in a relocation of the amide II peak from 1550 to 1450 cm^{-1} , while the amide I peak shifts by only $\sim 5\text{--}10 \text{ cm}^{-1}$. This provides a convenient monitor of the rate of exchange of hydrogen to deuterium by observing the disappearance of the amide II peak at 1550 cm^{-1} , thereby giving a measure of the global flexibility of a protein.^{81–83} Figure 6b shows the time-dependent change in the fraction of unexchanged hydrogen in lysozyme with different azoTAB concentrations and light conditions (see Experimental

Table 1. Analysis of H–D Exchange Kinetics of Lysozyme in the Presence of AzoTAB Surfactant

[azoTAB] (mM)	fast		slow		$\langle k \rangle (\times 10^4 \text{ min}^{-1})$
	percentage	$k (\times 10^2 \text{ min}^{-1})$	percentage	$k (\times 10^4 \text{ min}^{-1})$	
0	41	3.4	59	4.0	6.7
<i>trans</i>					
5	32	3.0	68	10	14
8	40	8.7	60	56	89
12	38	4.8	62	52	77
<i>cis</i>					
5	35	2.3	65	4.6	7.0
8	21	6.1	79	1.9	2.4
12	29	4.1	71	3.6	5.1

Procedures). In the presence of *trans* azoTAB, the protein is observed to exhibit an exchange rate faster than that of the native state, while *cis* azoTAB had little influence on the exchange rate. This implies that *trans* azoTAB induces enhanced protein flexibility relative to the native state, consistent with the NSE measurements described above.

The hydrogen atoms within a protein are usually divided into three groups: ultrafast-exchanging protons located on the surface of the protein, fast-exchanging protons contained within flexible structural elements, and slow-exchanging protons in the core of the protein formed by very rigid clusters.^{84,85} Ultrafast exchange is known to occur within a few seconds;⁸⁶ thus, only the fast and slow exchange processes can be observed in Figure 6 (the dead time of the FT-IR measurement is ≈ 2.5 min), with $\sim 50\%$ of the protons already exchanged at the earliest time points. Kinetic rates were obtained for the protein at each surfactant concentration by fitting the H–D exchange data to a biexponential decay function, with the results listed in Table 1. The rate constants of the fast-exchanging components within the protein are relatively constant at all azoTAB concentrations (both *trans* and *cis*). The exchange rate of the slow group, however, increases by ~ 1 order of magnitude when high concentrations of *trans* azoTAB are present (8×10^{-3} and 12×10^{-3} mol/L). In contrast, little change in the kinetic parameters relative to the native state was observed in the presence of *cis* azoTAB. The mean kinetic parameter $\langle k \rangle$, which provides a general measure of protein flexibility, also showed an enhanced exchange rate in the presence of *trans* azoTAB and relatively constant exchange rate for pure lysozyme and *cis* azoTAB–lysozyme complexes.

An increase in the H–D exchange rates results from destabilization of the secondary structure elements or unfolding of a compact core and, hence, a decrease in stability and/or rigidity and an increase in protein flexibility.^{72,81,83,87–89} The results presented in Figure 6 indicate that *trans* azoTAB induces an enhancement of lysozyme flexibility and dynamics, while *cis* azoTAB does not significantly change protein flexibility. Moreover, the dramatically enhanced slow-exchange rate constant and the largely unchanged fast-exchange rate constant of the *trans*-azoTAB–lysozyme complex may imply that the increased flexibility is due to protein swelling and destabilization of the protein core normally protected from solvent, while the fast-exchanging components in mobile flexible regions were not significantly influenced. The H–D exchange results are in agreement with the NSE measurements of enhanced protein domain motions in the presence of the *trans* isomer of azoTAB, as well as the SANS results indicating an increase in the radius of gyration (R_g) and an overall protein shape for lysozyme in

the presence of *trans* azoTAB, compared to nativelike conformations for lysozyme in the presence of *cis* azoTAB.

Previous studies have shown that lysozyme activity increases by nearly 1 order of magnitude in the presence of *trans* azoTAB surfactant relative to the native state.⁶³ From single-molecule FRET measurements³⁰ using identical dye pair locations as in Figure 5, the active cleft of native T4 lysozyme was found to exist in a relatively open conformation in the absence of substrate and in a relatively closed conformation when bound with the substrate. This demonstrates the necessity of hinge bending motions during enzymatic function. Similarly, a decrease in activity was observed for a lysozyme mutant in which residues near the hydrophobic core were replaced with more hydrophobic residues, which increased the stability and rigidity of the protein.⁹⁰ Additional studies using lysozyme mutants without residues Arg14 and His15 demonstrated enhanced enzyme activity with increases in enzyme flexibility relative to that of wild-type lysozyme.^{28,29} Thus, on the basis of the NSE measurements described above, the origin of azoTAB-induced superactivity of lysozyme could be the enhanced domain motions seen in the presence of the *trans* isomer of the surfactant.

CONCLUSIONS

Lysozyme dynamics induced by the photoresponsive azoTAB surfactant and light illumination have been examined using neutron spin echo combined with in vitro protein conformations determined with small-angle neutron scattering to study the protein structure–dynamics–function relationship. Shape reconstruction analysis applied to the SANS data indicates that the addition of *trans* azoTAB causes lysozyme to partially unfold relative to the native state, with swelling observed primarily away from the active site in the hinge region connecting the α and β domains. Upon illumination with UV light, *trans* azoTAB converts to the *cis* isomer, causing lysozyme to refold into a nativelike conformation. NSE experiments reveal enhanced dynamics of the partially unfolded lysozyme induced by *trans* azoTAB, while the nativelike lysozyme in the presence of *cis* azoTAB exhibited dynamics similar to that of a rigid body. Domain models employed to calculate the effective diffusion coefficient of the unfolded lysozyme consisting of either two or three domains give a good approximation of the enhanced protein dynamics induced by *trans* azoTAB. Ensemble-averaged FRET and H–D exchange measurements suggest that the protein exhibits higher flexibility induced by *trans* azoTAB, while the flexibility with *cis* azoTAB is similar to that of native lysozyme.

APPENDIX

Three models were employed to calculate the Q dependence of D_{eff} , including rigid-body analysis, a soft linker domain model proposed by Bu et al.,²⁶ and a freely jointed domain model proposed by Akcasu et al.⁷¹ The rigid-body model calculates the contributions of translation and rotational motions of rigid lysozyme to the Q -dependent oscillation of D_{eff} . The soft linker domain model assumes the protein to be composed of rigid domains connected by soft spring linkers where the first cumulant, the initial slope of the dynamic scattering function $\{\Omega(Q) = -\partial \ln[I(Q,t)/I(Q,0)]/\partial t\}$ is explicitly independent of the interdomain spring constant as assumed for soft linkages between domains. The freely jointed domain model treats the protein domains as n identical beads connected by freely rotating rigid bonds of length ζ . All models are available from the authors upon request.

Rigid-body calculations were applied to the crystal structure of lysozyme (PDB entry 6LYZ) and the solution structures of lysozyme-azoTAB complexes obtained from SANS by GA_STRUCT to account for translational and rotational motions through the equation²⁶

$$D_{\text{eff}}(Q) = \frac{k_B T}{Q^2} \times \frac{\sum_{jl} \langle b_j b_l [Q \mathbf{H}^T Q + \mathbf{L}(j) \mathbf{H}^R \mathbf{L}(l)] e^{iQ(r_j - r_l)} \rangle}{\sum_{jl} \langle b_j b_l e^{iQ(r_j - r_l)} \rangle} \tag{A1}$$

where b_j and b_l are neutron scattering lengths of effective scattering centers j and l , respectively. For the lysozyme crystal structure, the scattering centers were taken as each amino acid residue with the center of each residue being the average coordinate and the neutron scattering length of each residue being the sum of the neutron scattering lengths of all atoms in the residue. For the solution structure of lysozyme obtained by GA_STRUCT, b values were assumed to be identical for all scattering centers. $\mathbf{L}(j) = Qr_j$ is the angular momentum vector, while \mathbf{H}^T and \mathbf{H}^R are the translational and rotational mobility tensors, in which the three principle axis coefficients (D^T_x , D^T_y , and D^T_z in \mathbf{H}^T and D^R_x , D^R_y , and D^R_z in \mathbf{H}^R) were calculated with HYDROPRO.^{91,92}

In the soft linker domain model, the lysozyme molecule was divided into n rigid domains ($n = 2$ for a two-domain model, namely the α and β domains, or $n = 3$ for a three-domain model of the α and β domains and the hinge region). D_{eff} was calculated using the equation²⁶

$$D_{\text{eff}}(Q) = \frac{\sum_{i=1}^n D_i S_i}{S_{\text{Lys}}} \tag{A2}$$

where $D_i = (k_B T)/\xi_i$, with ξ_i being the friction constant of the i th domain. To obtain the results in Figure 4, it was necessary to increase the friction constant calculated from Kirkwood's formula²³ for each domain by a factor of 1.5. Similarly, Bu et al.²⁶ found it necessary to increase the friction coefficients of *Taq* polymerase domains by a factor of ≈ 2 , which is possibly caused by water displacement due to the proximity of the domains. S_i and S_{Lys} were obtained by the equation

$$S_i(Q) = \sum_{m,n \in i}^{N_i} \frac{\sin(Q|r_m - r_n|)}{Q|r_m - r_n|} \tag{A3}$$

which is the rotationally averaged static form factor of the i th domain with N_i being the number of scattering centers in the i th domain. S_{Lys} was calculated using an N of 1000, namely the total number of scattering centers in lysozyme.

The freely jointed domain model treats the protein as n rigid domains connected by $n - 1$ bonds of length ζ , with D_{eff} calculated from the equation⁷¹

$$D_{\text{eff}}(Q) = k_B T \frac{\mu(Q)}{S(Q)} \tag{A4}$$

where $S(Q)$ is the static scattering function given by

$$S(Q) = n \times \left\{ 1 + 2 \frac{n-1}{n} \frac{j_0(\zeta Q)}{1 - j_0(\zeta Q)} \times \left[1 - \frac{j_0(\zeta Q)}{1 - j_0(\zeta Q)} \frac{1 - j_0^{n-1}(\zeta Q)}{n-1} \right] \right\} \tag{A5}$$

and j_0 is the zeroth order spherical Bessel function. The mobility tensor $\mu(Q)$ is given by

$$\mu(Q) = \mu_1(Q) - \mu_2(Q) \tag{A6}$$

where

$$\mu_1(Q) = j_0(\zeta Q)^{|\mu-\nu|} H_{\mu\nu} \tag{A7}$$

and

$$\mu_2(Q) = \frac{\xi}{2\zeta^2(1-\tau)} \sum_{\mu,\nu=1}^n \sum_{j=1}^{n-1} [\mathbf{HC}]_{\mu j} \times \langle e^{iQR_{\mu\nu}(Q\zeta_j)^2} \rangle [\mathbf{C}^T \mathbf{H}]_{j\nu} \tag{A8}$$

In these equations \mathbf{H} is the preaveraged hydrodynamic interaction matrix given by

$$\mathbf{H}_{\mu\nu} = \frac{1}{\xi} \left[\delta_{\mu\nu} + (1 - \delta_{\mu\nu}) \tau \frac{2}{\pi} \int_0^\infty dx j_0(x)^{|\mu-\nu|} \right] \tag{A9}$$

and $\tau = \xi/6\pi\zeta\eta$ is the draining parameter determined by friction constant ξ , solvent viscosity η , and bond length ζ . \mathbf{C} is an $n - 1 \times n$ matrix defined by

$$\mathbf{C}_{\mu j} = \delta_{\mu j} - \delta_{\mu, j-1} \tag{A10}$$

where δ is the Kronecker delta. The indices μ and ν run over all protein domains (from 1 to n), while the index j runs over all bonds (from 1 to $n - 1$). The ensemble average is approximated as

$$\langle e^{iQR_{\mu\nu}(Q\zeta_j)^2} \rangle = \zeta^2 j_0(Q\zeta)^{|\mu-\nu|-1} \times \left[j_0(Q\zeta) - \frac{2j_1(Q\zeta)}{Q\zeta} \right] \tag{A11}$$

when $|\mu - \nu| = 1$ and $\mu = j + 1$ or $\nu = j + 1$; otherwise

$$\langle e^{iQR_{\mu\nu}(Q\zeta_j)^2} \rangle = \frac{\zeta^2}{3} j_0(Q\zeta)^{|\mu-\nu|} \tag{A12}$$

To apply the freely jointed domain model, we divided lysozyme into $n = 3$ domains, representing the α and β domains and the hinge region, connected by $n - 1 = 2$ bonds. The

approximate center of mass of each domain was visually selected from the PDB file produced by GA_STRUCT, while each scattering center was associated with the closest domain. Bond length ζ was taken as the average distance between the centers of mass of the three domains (25 Å), while the friction constant was taken as the average value calculated from the Kirkwood formula of the three individual domains, again increased by a factor of 1.5 to account for an ≈ 3 Å thick hydration layer around each domain.^{65,94}

AUTHOR INFORMATION

Corresponding Author

*Phone: (213) 740-2066. Fax: (213) 740-8053. E-mail: tedlee@usc.edu.

Funding

This material is based upon work supported by National Science Foundation Grant 0554115.

Notes

The identification of any commercial product or trade name does not imply endorsement or recommendation by the National Institute of Standards and Technology.

ACKNOWLEDGMENTS

We acknowledge the generous advice and instruction of Dr. Boualem Hammouda with respect to domain motion analysis. This work utilized facilities supported in part by National Science Foundation Grant DMR-0454672. We acknowledge the support of the National Institute of Standards and Technology, U.S. Department of Commerce, in providing the neutron research facilities used in this work.

REFERENCES

- (1) Bendedouch, D., and Chen, S. H. (1983) Structure and interparticle interactions of bovine serum albumin in solution studied by small-angle neutron scattering. *J. Phys. Chem.* 87, 1473–1477.
- (2) Zhang, X.-j., Wozniak, J. A., and Matthews, B. W. (1995) Protein flexibility and adaptability seen in 25 crystal forms of T4 lysozyme. *J. Mol. Biol.* 250, 527–552.
- (3) Johnson, L. N., and Phillips, D. C. (1965) Structure of some crystalline lysozyme-inhibitor complexes determined by X-ray analysis at 6 Å resolution. *Nature* 206, 761–763.
- (4) Meinhold, L., and Smith, J. C. (2007) Protein dynamics from X-ray crystallography: Anisotropic, global motion in diffuse scattering patterns. *Proteins: Struct., Funct., Bioinf.* 66, 941–953.
- (5) Agarwal, P. K. (2006) Enzymes: An integrated view of structure, dynamics and function. *Microb. Cell Fact.* 5, 2.
- (6) Daniel, R. M., Dunn, R. V., Finney, J. L., and Smith, J. C. (2003) The role of dynamics in enzyme activity. *Annu. Rev. Biophys. Biomol. Struct.* 32, 69–92.
- (7) Ishima, R., and Torchia, D. A. (2000) Protein dynamics from NMR. *Nat. Struct. Biol.* 7, 740–743.
- (8) Palmer, A. G. III (2004) NMR characterization of the dynamics of biomacromolecules. *Chem. Rev.* 104, 3623–3640.
- (9) Osborne, M. J., Schnell, J., Benkovic, S. J., Dyson, H. J., and Wright, P. E. (2001) Backbone dynamics in dihydrofolate reductase complexes: Role of loop flexibility in the catalytic mechanism. *Biochemistry* 40, 9846–9859.
- (10) Barre, P., Zschoernig, O., Arnold, K., and Huster, D. (2003) Structural and Dynamical Changes of the Bindin B18 Peptide upon Binding to Lipid Membranes. A Solid-State NMR Study. *Biochemistry Eng.* 7, 743–748.
- (11) Bouvignies, G., Bernado, P., Meier, S., Cho, K., Grzesiek, S., Bruschweiler, R., and Blackledge, M. (2005) Identification of slow correlated motions in proteins using residual dipolar and hydrogen-bond scalar couplings. *Proc. Natl. Acad. Sci. U.S.A.* 102, 13885–13890.
- (12) Nandi, N., Bhattacharyya, K., and Bagchi, B. (2000) Dielectric Relaxation and Solvation Dynamics of Water in Complex Chemical and Biological Systems. *Chem. Rev.* 100, 2013–2045.
- (13) Fenimore, P. W., Frauenfelder, H., McMahon, B. H., and Parak, F. G. (2002) Slaving: Solvent fluctuations dominate protein dynamics and functions. *Proc. Natl. Acad. Sci. U.S.A.* 99, 16047–16051.
- (14) Jansson, H., Bergman, R., and Swenson, J. (2005) Relation between Solvent and Protein Dynamics as Studied by Dielectric Spectroscopy. *J. Phys. Chem. B* 109, 24134–24141.
- (15) Pawlus, S., Khodadadi, S., and Sokolov, A. P. (2008) Conductivity in Hydrated Proteins: No Signs of the Fragile-to-Strong Crossover. *Phys. Rev. Lett.* 100, 108103/1–108103/4.
- (16) Khodadadi, S., Pawlus, S., and Sokolov, A. P. (2008) Influence of hydration on protein dynamics: Combining dielectric and neutron scattering spectroscopy data. *J. Phys. Chem. B* 112, 14273–14280.
- (17) Frauenfelder, H., Chen, G., Berendzen, J., Fenimore, P. W., Jansson, H., McMahon, B. H., Strope, I. R., Swenson, J., and Young, R. D. (2009) A unified model of protein dynamics. *Proc. Natl. Acad. Sci. U.S.A.* 106, 5129–5134.
- (18) Cummins, H. Z. (1974) in *Photon Correlation and Light Beating Spectroscopy* (Cummins, H. Z., and Pike, E. R., Eds.) p 313, Plenum, New York.
- (19) Phillies, G. D. J., Benedek, G. B., and Mazer, N. A. (1976) Diffusion in protein solutions at high concentrations: A study by quasielastic light scattering spectroscopy. *J. Chem. Phys.* 65, 1883–1892.
- (20) Burchard, W. (1992) in *Laser Light Scattering in Biochemistry* (Harding, S. E., Sattelle, D. B., and Bloomfield, V. A., Eds.) pp 3–22, Royal Society of Chemistry, Cambridge, U.K.
- (21) Berne, B. J., and Pecora, R. (2000) in *Dynamic Light Scattering with Applications to Chemistry, Biology and Physics*, Dover, New York.
- (22) Hess, S. T., Huang, S., Heikal, A. A., and Webb, W. W. (2002) Biological and Chemical Applications of Fluorescence Correlation Spectroscopy: A Review. *Biochemistry* 41, 697–705.
- (23) Gabel, F., Bicut, D., Lehnert, U., Tehei, M., Weik, M., and Zaccai, G. (2002) Protein dynamics studied by neutron scattering. *Q. Rev. Biophys.* 35, 327–367.
- (24) Liu, D., Chu, X.-q., Lagi, M., Zhang, Y., Fratini, E., Baglioni, P., Alatas, A., Said, A., Alp, E., and Chen, S.-H. (2008) Studies of Phononlike Low-Energy Excitations of Protein Molecules by Inelastic X-ray Scattering. *Phys. Rev. Lett.* 101, 135501/1–135501/4.
- (25) Hayward, S., Kitao, A., and Berendsen, H. J. C. (1997) Model-free methods of analyzing domain motions in proteins from simulation: A comparison of normal mode analysis and molecular dynamics simulation of lysozyme. *Proteins: Struct., Funct., Genet.* 27, 425–437.
- (26) Bu, Z., Bieh, R., Monkenbusch, M., Richter, D., and Callaway, D. J. E. (2005) Coupled protein domain motion in Taq polymerase revealed by neutron spin-echo spectroscopy. *Proc. Natl. Acad. Sci. U.S.A.* 102, 17646–17651.
- (27) Arnold, G. E., and Ornstein, R. L. (1997) Protein hinge bending as seen in molecular dynamics simulations of native and M6I mutant T4 lysozymes. *Biopolymers* 41, 533–544.
- (28) Mine, S., Tate, S., Ueda, T., Kainosho, M., and Imoto, T. (1999) Analysis of the relationship between enzyme activity and its internal motion using nuclear magnetic resonance: ¹⁵N relaxation studies of wild-type and mutant lysozyme. *J. Mol. Biol.* 286, 1547–1565.
- (29) Imoto, T., Ueda, T., Tamura, T., Isakari, Y., Abe, Y., Inoue, M., Miki, T., Kawano, K., and Yamada, H. (1994) Lysozyme requires fluctuation of the active site for the manifestation of activity. *Protein Eng.* 7, 743–748.

- (30) Chen, Y., Hu, D., Vorpapel, E. R., and Lu, H. P. (2003) Probing Single-Molecule T4 Lysozyme Conformational Dynamics by Intramolecular Fluorescence Energy Transfer. *J. Phys. Chem. B* 107, 7947–7956.
- (31) Farago, B. (2006) Neutron spin echo study of well organized soft matter systems. *Phys. B (Amsterdam, Neth.)* 385–386, 688–691.
- (32) Hellweg, T., Gradzielski, M., Farago, B., and Langevin, D. (2001) Shape fluctuations of microemulsion droplets: A neutron spin-echo study. *Colloids Surf., A* 183–185, 159–169.
- (33) Komura, S., Takeda, T., Seto, H., and Nagao, M. (2003) Dynamical fluctuation of cylindrical micelles and membranes in binary and ternary amphiphilic microemulsion systems. *Lect. Notes Phys.* 601, 302–311.
- (34) Monkenbusch, M. (2003) Soft matter and biology. *Lect. Notes Phys.* 601, 246–267.
- (35) Richter, D., Monkenbusch, M., Arbe, A., and Colmenero, J. (2001) Neutron scattering and the glass transition in polymers: Present status and future opportunities. *J. Non-Cryst. Solids* 287, 286–296.
- (36) Doster, W., Cusack, S., and Petry, W. (1989) Dynamical transition of myoglobin revealed by inelastic neutron scattering. *Nature* 337, 754–756.
- (37) Haussler, W., and Farago, B. (2003) Diffusive dynamics of ordered solutions of apoferritin near the structure factor peak. *J. Phys.: Condens. Matter* 15, S197–S204.
- (38) Doster, W., and Longeville, S. (2007) Microscopic diffusion and hydrodynamic interactions of hemoglobin in red blood cells. *Biophys. J.* 93, 1360–1368.
- (39) Le Coeur, C., and Longeville, S. (2008) Microscopic protein diffusion at high concentration by neutron spin-echo spectroscopy. *Chem. Phys.* 345, 298–304.
- (40) Longeville, S., Doster, W., and Kali, G. (2003) Myoglobin in crowded solutions: Structure and diffusion. *Chem. Phys.* 292, 413–424.
- (41) Porcar, L., Falus, P., Chen, W.-R., Faraone, A., Fratini, E., Hong, K., Baglioni, P., and Liu, Y. (2010) Formation of the Dynamic Clusters in Concentrated Lysozyme Protein Solutions. *J. Phys. Chem. Lett.* 1, 126–129.
- (42) Zanotti, J.-M., Bellissent-Funel, M.-C., and Parello, J. (1999) Hydration-coupled dynamics in proteins studied by neutron scattering and NMR: The case of the typical EF-hand calcium-binding parvalbumin. *Biophys. J.* 76, 2390–2411.
- (43) Perez, J., Zanotti, J.-M., and Durand, D. (1999) Evolution of the internal dynamics of two globular proteins from dry powder to solution. *Biophys. J.* 77, 454–469.
- (44) Zaccai, G. (2000) How Soft Is a Protein? A Protein Dynamics Force Constant Measured by Neutron Scattering. *Science* 288, 1604–1607.
- (45) Tsai, A. M., Neumann, D. A., and Bell, L. N. (2000) Molecular dynamics of solid-state lysozyme as affected by glycerol and water: A neutron scattering study. *Biophys. J.* 79, 2728–2732.
- (46) Chen, S.-H., Liu, L., Fratini, E., Baglioni, P., Faraone, A., and Mamontov, E. (2006) Observation of fragile-to-strong dynamic crossover in protein hydration water. *Proc. Natl. Acad. Sci. U.S.A.* 103, 9012–9016.
- (47) Khodadadi, S., Pawlus, S., Roh, J. H., Garcia Sakai, V., Mamontov, E., and Sokolov, A. P. (2008) The origin of the dynamic transition in proteins. *J. Chem. Phys.* 128, 195106/1–195106/5.
- (48) Zhang, Y., Lagi, Ma., Liu, D., Mallamace, F., Fratini, E., Baglioni, P., Mamontov, E., Hagen, M., and Chen, S.-H. (2009) Observation of high-temperature dynamic crossover in protein hydration water and its relation to reversible denaturation of lysozyme. *J. Chem. Phys.* 130, 135101/1–135101/8.
- (49) Doster, W., Busch, S., Gaspar, A. M., Appavou, M. S., Wuttke, J., and Scheer, H. (2010) Dynamical transition of protein-hydration water. *Phys. Rev. Lett.* 104, 098101.
- (50) Wood, K., Lehnert, U., Kessler, B., Zaccai, G., and Oesterhelt, D. (2008) Hydration dependence of active core fluctuations in bacteriorhodopsin. *Biophys. J.* 95, 194–202.
- (51) Weik, M., Lehnert, U., and Zaccai, G. (2005) Liquid-like water confined in stacks of biological membranes at 200 K and its relation to protein dynamics. *Biophys. J.* 89, 3639–3646.
- (52) Lehnert, U., Reat, V., Weik, M., Zaccai, G., and Pfister, C. (1998) Thermal motions in bacteriorhodopsin at different hydration levels studied by neutron scattering: Correlation with kinetics and light-induced conformational changes. *Biophys. J.* 75, 1945–1952.
- (53) Rheinstädter, M. C., Schmalzl, K., Wood, K., and Strauch, D. (2009) Protein-Protein Interaction in Purple Membrane. *Phys. Rev. Lett.* 103, 128104/1–128104/4.
- (54) Wood, K., Plazanet, M., Gabel, F., Kessler, B., Oesterhelt, D., Tobias, D. J., Zaccai, G., and Weik, M. (2007) Coupling of protein and hydration-water dynamics in biological membranes. *Proc. Natl. Acad. Sci. U.S.A.* 104, 18049–18054.
- (55) Busch, S., Smuda, C., Pardo, L. C., and Unruh, T. (2010) Molecular Mechanism of Long-Range Diffusion in Phospholipid Membranes Studied by Quasielastic Neutron Scattering. *J. Am. Chem. Soc.* 132, 3232–3233.
- (56) Rheinstädter, M.C., Das, J., Flenner, E. J., Bruning, B., Seydel, T., and Kosztin, I. (2008) Motional Coherence in Fluid Phospholipid Membranes. *Phys. Rev. Lett.* 101, 248106/1–248106/4.
- (57) Fitter, J., Verclas, S. A. W., Lechner, R. E., Buldt, G., Ernst, O. P., Hofmann, K. P., and Dencher, N. A. (1999) Bacteriorhodopsin and rhodopsin studied by incoherent neutron scattering: Dynamical properties of ground states and light activated intermediates. *Phys. B (Amsterdam, Neth.)* 266, 35–40.
- (58) Pieper, J. (2010) Time-resolved quasielastic neutron scattering studies of native photosystems. *Biochim. Biophys. Acta* 1804, 83–88.
- (59) Furrer, A., and Stockli, A. (2010) Inelastic neutron scattering study of light-induced dynamics of a photosynthetic membrane system. *Phys. Rev. E: Stat., Nonlinear, Soft Matter Phys.* 81, 011901/1–011901/5.
- (60) Biehl, R., Hoffmann, B., Monkenbusch, M., Falus, P., Preost, S., Merkel, R., and Richter, D. (2008) Direct Observation of Correlated Interdomain Motion in Alcohol Dehydrogenase. *Phys. Rev. Lett.* 101, 138102/1–138102/4.
- (61) Farago, B., Li, J.-Q., Cornilescu, G., Callaway, D. J. E., and Bu, Z.-M. (2010) Activation of Nanoscale Allosteric Protein Domain Motion Revealed by Neutron Spin Echo Spectroscopy. *Biophys. J.* 99, 3473–3482.
- (62) Inoue, R., Biehl, R., Rosenkranz, T., Fitter, J., Monkenbusch, M., Radulescu, A., Farago, B., and Richter, D. (2010) Large Domain Fluctuations on 50-ns Timescale Enable Catalytic Activity in Phosphoglycerate Kinase. *Biophys. J.* 99, 2309–2317.
- (63) Wang, S.-C., and Lee, C. T. Jr. (2007) Enhanced Enzymatic Activity through Photoreversible Conformational Changes. *Biochemistry* 46, 14557–14566.
- (64) Hayashita, T., Kurosawas, T., Miyata, T., Tanaka, K., and Igawa, M. (1994) Effect of structural variation within cationic azo-surfactant upon photoresponsive function in aqueous solution. *Colloid Polym. Sci.* 272, 1611–1619.
- (65) Hamill, A. C., Wang, S.-C., and Lee, C. T. Jr. (2005) Probing lysozyme conformation with light reveals a new folding intermediate. *Biochemistry* 44, 15139–15149.
- (66) Glinka, C. J., Barker, J. G., Hammouda, B., Krueger, S., Moyer, J. J., and Orts, W. J. (1998) The 30 m small-angle neutron scattering instruments at the National Institute of Standards and Technology. *J. Appl. Crystallogr.* 31, 430–445.
- (67) Svergun, D. I., Petoukhov, M. V., and Koch, M. H. (2001) Determination of domain structure of proteins from X-ray solution scattering. *Biophys. J.* 80, 2946–2953.

- (68) Heller, W. T., Krueger, J. K., and Trewella, J. (2003) Further Insights into Calmodulin-Myosin Light Chain Kinase Interaction from Solution Scattering and Shape Restoration. *Biochemistry* 42, 10579–10588.
- (69) Rosov, N., Rathgeber, S., and Monkenbusch, M. (2000) in *Scattering from polymers: Characterization by X-rays, neutrons, and light* (Cebe, P., Hsiao, B. S., and Lohse, D. J., Eds.) ACS Symposium Series 739, pp 103–116, American Chemical Society, Washington, DC.
- (70) Azuah, R. T., Kneller, L. R., Qiu, Y., Tregenna-Piggott, P. L. W., Brown, C. M., Copley, J. R. D., and Dimeo, R. M. (2009) DAVE: A comprehensive software suite for the reduction, visualization, and analysis of low energy neutron spectroscopic data. *J. Res. Natl. Inst. Stand. Technol.* 114, 341–358.
- (71) Akcasu, A. Z., Hammouda, B., Stockmayer, W. H., and Tanaka, G. (1986) First cumulant for chains with constraints. *J. Chem. Phys.* 85, 4734–4743.
- (72) Heimburg, T., and Marsh, D. (1993) Investigation of secondary and tertiary structural changes of cytochrome c in complexes with anionic lipids using amide hydrogen exchange measurements: An FTIR study. *Biophys. J.* 65, 2408–2417.
- (73) Wang, D., and Geva, E. (2005) Protein structure and dynamics from single-molecule fluorescence resonance energy transfer. *J. Phys. Chem. B* 109, 1626–1634.
- (74) Stenstam, A., Montalvo, G., Grillo, I., and Gradzielski, M. (2003) Small Angle Neutron Scattering Study of Lysozyme-Sodium Dodecyl Sulfate Aggregates. *J. Phys. Chem. B* 107, 12331–12338.
- (75) Gebe, J. A., and Schurr, J. M. (1993) Intramolecular interference effects in dynamic light scattering from rigid rings. *Biopolymers* 33, 1757–1764.
- (76) Haliloglu, T., and Bahar, I. (1999) Structure-based analysis of protein dynamics: Comparison of theoretical results for hen lysozyme with X-ray diffraction and NMR relaxation data. *Proteins: Struct., Funct., Genet.* 37, 654–667.
- (77) Kuroki, R., Weaver, L. H., and Matthews, B. W. (1993) A covalent enzyme-substrate intermediate with saccharide distortion in a mutant T4 lysozyme. *Science* 262, 2030–2033.
- (78) Vigano, C., Smeyers, M., Raussens, V., Scheirlinckx, F., Ruyschaert, J. M., and Goormaghtigh, E. (2004) Hydrogen-deuterium exchange in membrane proteins monitored by IR spectroscopy: A new tool to resolve protein structure and dynamics. *Biopolymers* 74, 19–26.
- (79) Grimard, V., Vigano, C., Margolles, A., Wattiez, R., van Veen, H. W., Konings, W. N., Ruyschaert, J. M., and Goormaghtigh, E. (2001) Structure and dynamics of the membrane-embedded domain of LmrA investigated by coupling polarized ATR-FTIR spectroscopy and $^1\text{H}/^2\text{H}$ exchange. *Biochemistry* 40, 11876–11886.
- (80) Raussens, V., Narayanaswami, V., Goormaghtigh, E., Ryan, R. O., and Ruyschaert, J. M. (1996) Hydrogen/deuterium exchange kinetics of apolipoprotein III in lipid-free and phospholipid-bound states. An analysis by Fourier transform infrared spectroscopy. *J. Biol. Chem.* 271, 23089–23095.
- (81) Kohen, A., and Klinman, J. P. (2000) Protein Flexibility Correlates with Degree of Hydrogen Tunneling in Thermophilic and Mesophilic Alcohol Dehydrogenases. *J. Am. Chem. Soc.* 122, 10738–10739.
- (82) Liang, Z.-X., Tsigos, I., Lee, T., Bouriotis, V., Resing, K. A., Ahn, N. G., and Klinman, J. P. (2004) Evidence for Increased Local Flexibility in Psychrophilic Alcohol Dehydrogenase Relative to Its Thermophilic Homologue. *Biochemistry* 43, 14676–14683.
- (83) Celej Maria, S., Montich Guillermo, G., and Fidelio Gerardo, D. (2003) Protein stability induced by ligand binding correlates with changes in protein flexibility. *Protein Sci.* 12, 1496–1506.
- (84) Vigano, C., Goormaghtigh, E., and Ruyschaert, J. M. (2003) Detection of structural and functional asymmetries in P-glycoprotein by combining mutagenesis and H/D exchange measurements. *Chem. Phys. Lipids* 122, 121–135.
- (85) Gekko, K., Obu, N., Li, J., and Lee, J. C. (2004) A linear correlation between the energetics of allosteric communication and protein flexibility in the *Escherichia coli* cyclic AMP receptor protein revealed by mutation-induced changes in compressibility and amide hydrogen-deuterium exchange. *Biochemistry* 43, 3844–3852.
- (86) Kossiakoff, A. A., and Spencer, S. A. (1980) Neutron diffraction identifies histidine-57 as the catalytic base in trypsin. *Nature* 288, 414–416.
- (87) Scheirlinckx, F., Buchet, R., Ruyschaert, J.-M., and Goormaghtigh, E. (2001) Monitoring of secondary and tertiary structure changes in the gastric H^+/K^+ -ATPase by infrared spectroscopy. *Eur. J. Biochem.* 268, 3644–3653.
- (88) de Jongh, H. H. J., Goormaghtigh, E., and Ruyschaert, J.-M. (1995) Tertiary stability of native and methionine-80 modified cytochrome c detected by proton-deuterium exchange using online Fourier transform infrared spectroscopy. *Biochemistry* 34, 172–179.
- (89) Celej, M. S., Montich, G. G., and Fidelio, G. D. (2004) Conformational flexibility of avidin: The influence of biotin binding. *Biochem. Biophys. Res. Commun.* 325, 922–927.
- (90) Ohmura, T., Ueda, T., Ootsuka, K., Saito, M., and Imoto, T. (2001) Stabilization of hen egg white lysozyme by a cavity-filling mutation. *Protein Sci.* 10, 313–320.
- (91) De la Torre, J. G., Huertas, M. L., and Carrasco, B. (2000) Calculation of hydrodynamic properties of globular proteins from their atomic-level structure. *Biophys. J.* 78, 719–730.
- (92) Carrasco, B., and De la Torre, J. G. (1999) Hydrodynamic properties of rigid particles: Comparison of different modeling and computational procedures. *Biophys. J.* 76, 3044–3057.
- (93) Kirkwood, J. G. (1954) The general theory of irreversible processes in solutions of macromolecules. *J. Polym. Sci.* 12, 1–14.
- (94) Lee, C. T. Jr., Smith, K. A., and Hatton, T. A. (2005) Photocontrol of Protein Folding: The Interaction of Photosensitive Surfactants with Bovine Serum Albumin. *Biochemistry* 44, 524–536.